Revisiting 1-hexene low-temperature oxidation

Xiangzan Meng[1,2], Anne Rodriguez[1], Olivier Herbinet[1], Tianyou Wang[2],

Frédérique Battin-Leclerc[1*]

[1]Laboratoire Réactions et Génie des Procédés, CNRS, Université de Lorraine, Nancy, France

[2]State Key Laboratory of Engines, Tianjin University, Tianjin 300072, China

SUPPLEMENTARY DESCRIPTION

[*]Corresponding author. Frédérique Battin-Leclerc: E-mail: frederique.battin-leclerc@univ-lorraine.fr, Phone: +33 3 83 17 51 25, Fax: +33 3 83 37 81 20

1/ Additional details about the used experimental devices and methods

1a/ Schemes of the apparatuses coupling JSR to time-of-flight mass spectrometer combined with laser photoionization

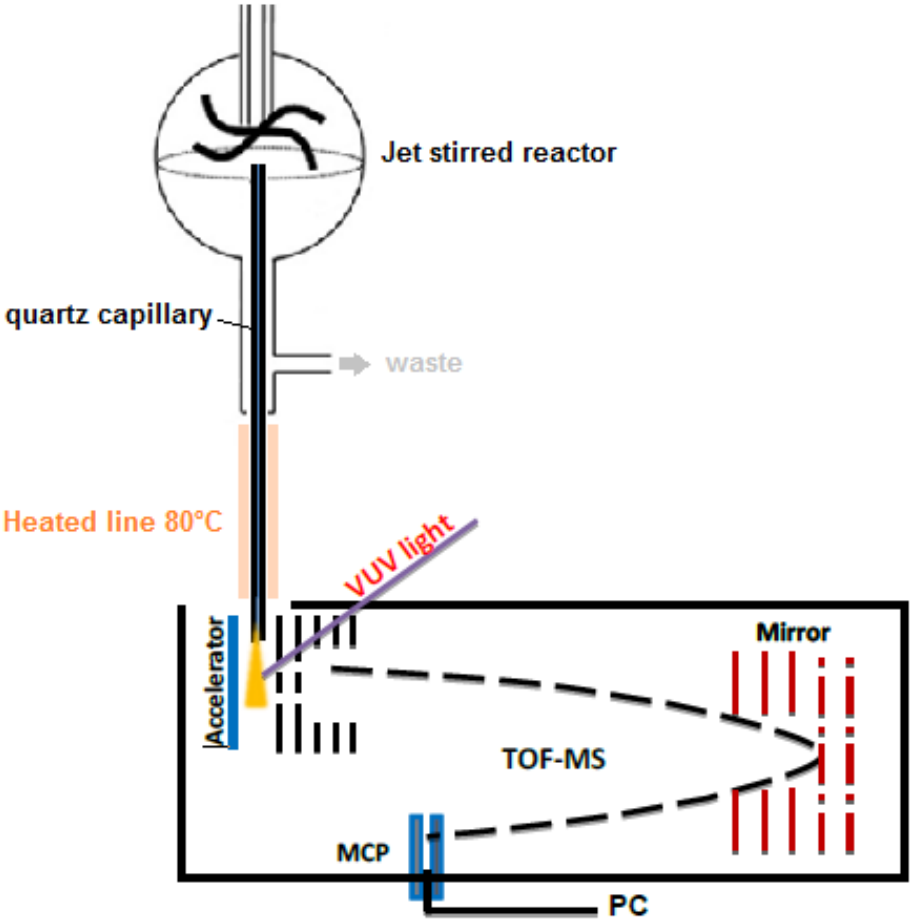

Figure S1: Schematic diagram of the instruments including the jet-stirred reactor and the laser photoionization mass spectrometer.

1b/ Method used for calculating mole fraction from mass spectrometer ion signal

As shown previously [1], for time-of-flight mass spectrometry combined with laser ionization with capillary tube sampling, the mole fraction of a species of mass i can be obtained from that of a reference species, of mass ref, at a given temperature and the laser energy by the simplified equation (1):

$$\frac{S_i(T)}{S_{ref}(T)} = \frac{X_i(T)}{X_{ref}(T)} \cdot \frac{\sigma_i(T)}{\sigma_{ref}(T)} \quad (1)$$

Cross sections used for the quantification of species detected by mass spectrometry

As a reminder, the following ionization energy has been used: 10.6 eV.

Compound name	Formula	m/z	IE (eV)	σ (Mb) at 10.6 eV	Reference
Hexenyl-ketohydroperoxide	$C_6H_{10}O_3$	130	Not determined	15.32	*Estimated**
Hexenyl-hydroperoxide	$C_6H_{12}O_2$	116	≈9.2	17.89	*Estimated**
Butenyl-hydroperoxide	$C_4H_8O_2$	88	9.29	16.43	*Estimated**
Propyl-hydroperoxide	$C_3H_8O_2$	76	9.53	5.80	*Estimated**
Allyl-hydroperoxide	$C_3H_6O_2$	74	9.55	15.71	*Estimated**
Ethyl-hydroperoxide	$C_2H_6O_2$	62	9.61	5.07	*Estimated**
Methyl-hydroperoxide	CH_4O_2	48	9.84	4.35	*Estimated**
Acetaldehyde	C_2H_4O	44	10.229	8.06	*Cool et al. [4]*
Propene	C_3H_6	42	9.73	11.36	*Cool et al. [4]*
Ketene	C_2H_2O	42	9.62	22.52	*Yang et al. [5]*

** see below for the method used the estimation of cross sections*

Method for the estimation of cross sections

For compounds for which we haven't found the cross section in the literature, we had to make an estimate. This estimation method is based on the group additivity method proposed by Bobeldijk et al. [9]. Groups are defined as atom pairs in the considered molecules.

The value of each group is estimated from published data of known species at a given photon energy. From there, we simply sum each group constituting the related molecule in order to estimate its cross section.

cross section of atom pairs at 10.6 eV

group	σ (Mb)	compound	Reference
C-C or O-O	0.7275	*n*-pentane	*Zhou et al. [3]*
C=C	10.633	Propene	*Cool et al. [4]*
C-O	4.345	Dimethyl-ether	*Cool et al. [7]*
C=O	7.3325	Acetaldehyde	*Cool et al. [4]*
C-H or O-H	0		

1c/ Description of the cw-CRDS analyses and the related quantification method

As described by Bahrini et al. [11], the near-infrared beam was provided by a fibred distributed feed-back (DFB) diode laser (Fitel-Furukawa FOL15DCWB-A81-W1509) emitting up to 40 mW, the wavelength can be varied in the range 6640±13 cm^{-1} through changing the current applied to the diode laser. The diode laser emission is directly fibred and passes through a fibred optical isolator and a fibred acousto-optical modulator (AOM, AA Opto-Electronic). The AOM allows the laser beam to be deviated within 350 ns with respect to a trigger signal for a total duration of 1.5 ms. The zero-order beam is connected to a fibred optical wave meter (228 Bristol Instruments) for monitoring the wavelength of the laser emission with an accuracy of 0.01 cm^{-1}. The main first-order laser beam is coupled into the CRDS optical cavity through a short-focal-length lens (f = 10 mm) for mode matching so as to excite the fundamental TEM_{00} mode. Two folding micrometric mirrors allow easy alignment of the beam, as shown in Figure S2. The flow rate in the cell is 0.25 L/min, while the total flow rate in the reactor is about 1 L/min.

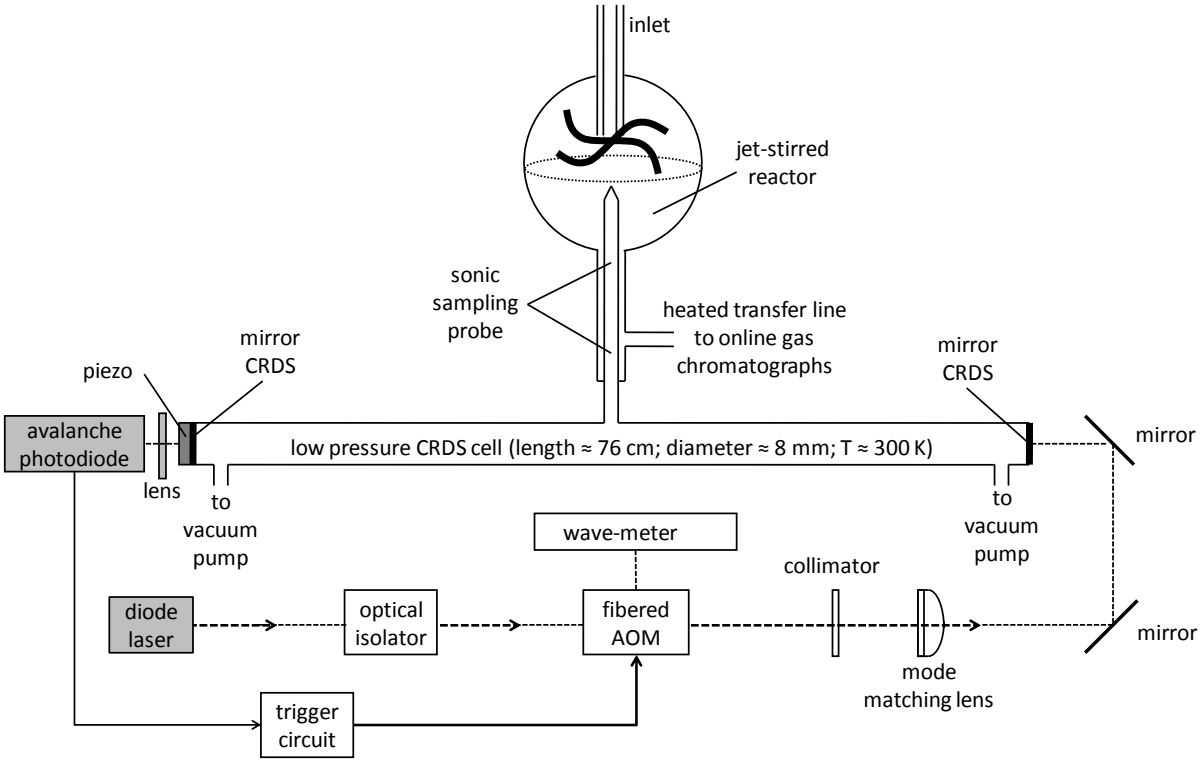

Figure S2: Schematic view of the experimental set-up (AOM= Acousto-optical modulator).

After many round trips, the optical signal transmitted through the cavity is converted into current by an avalanche photodiode (Perkin Elmer C30662E). A lab-designed amplifier-threshold circuit converts the current signal to an exploitable voltage signal and triggers the AOM to deviate the laser beam (turn off of the first order) as soon as the cavity comes into resonance and the photodiode signal is connected to a fast 16-bit analogue acquisition card (PCI-6259, National Instruments) in a PC, which is triggered also by the amplifier-threshold circuit. The acquisition card has an acquisition frequency of 1.25 MHz, and thus the ring-down signal is sampled every 800 ns and the data are transferred to PC in real time. The ring-down time τ is obtained by fitting the exponential decay over a time range of seven lifetimes by a Levenberg-Marquardt exponential fit in LabView.

The concentration of a species being formed or consumed during the hydrocarbon oxidation process in a jet-stirred reactor (JSR), can be obtained by measuring the ring-down time of the empty cavity τ_0 (i.e., the ring-down time before heating the reactor) and the ring-down time τ, when performing an experiment at a given temperature:

$$\alpha = [A] \times \sigma = \frac{R_L}{c}\left(\frac{1}{\tau} - \frac{1}{\tau_0}\right) \quad (1)$$

where σ is the absorption cross section, R_L is the ratio between the cavity length L (i.e., the distance between the two cavity mirrors to the length L_A over which the absorber is present; see section on CH_4 quantification), and c is the speed of light. Knowing the absorption cross section σ, one can extract the concentration *[A]* of the target molecule.

Table S1: Absorption lines and cross sections used for the quantification of formaldehyde, water, hydrogen peroxide and ethylene.

	wavenumber υ (cm^{-1})	**cross section σ (cm^2)**	**reference**
CH_2O	6639.33	3.60×10^{-22}	Morajkar et al. [12]
	6641.67	4.59×10^{-22}	
H_2O	6638.9*****	4.46×10^{-23}	Macko et al. [13]
	6640.9	1.60×10^{-22}	
	6641.27*****	1.82×10^{-22}	
H_2O_2	6639.26	7.62×10^{-23}	Parker et al. [14]
	6640.06	1.41×10^{-22}	
C_2H_4	6638.33	4.05×10^{-23}	Bahrini et al. [11]
	6641.23	2.95×10^{-23}	

***** These lines were used only at high temperature because they were perturbed by another peak at low-temperature resulting in uncertainties.

2/ Pathways involved during OH radical addition to 1-hexene

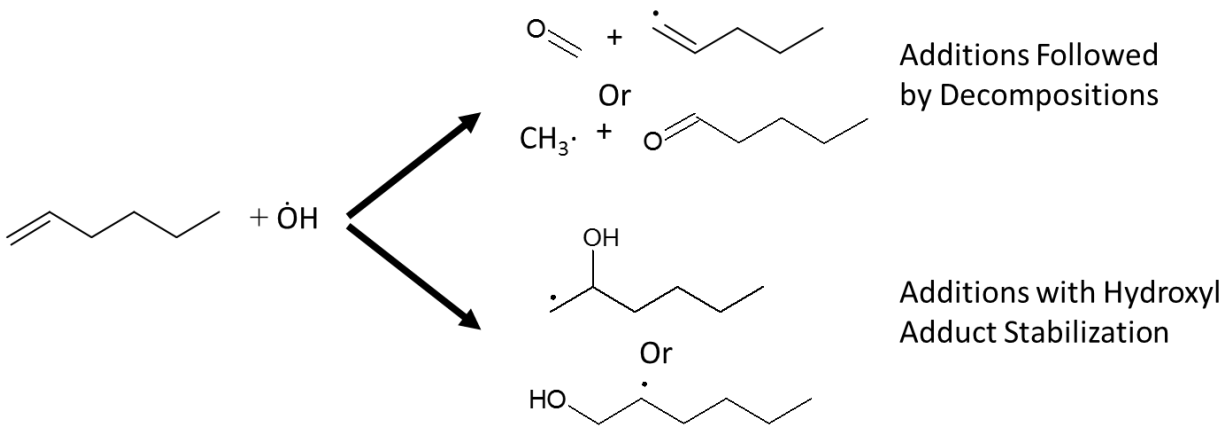

Figure S3: Pathways involved during OH radical addition to 1-hexene.

3/ Modeling of high-temperature oxidation literature data

** JSR results at high pressure*

Figures S3 and S4 demonstrate that the current model reproduces well the data obtained during the high pressure JSR experiments conducted by Yahyaoui et al. [15]. The current model correctly describes the fuel reactivity and the product formation at both studied equivalence ratios (0.5 and 1).

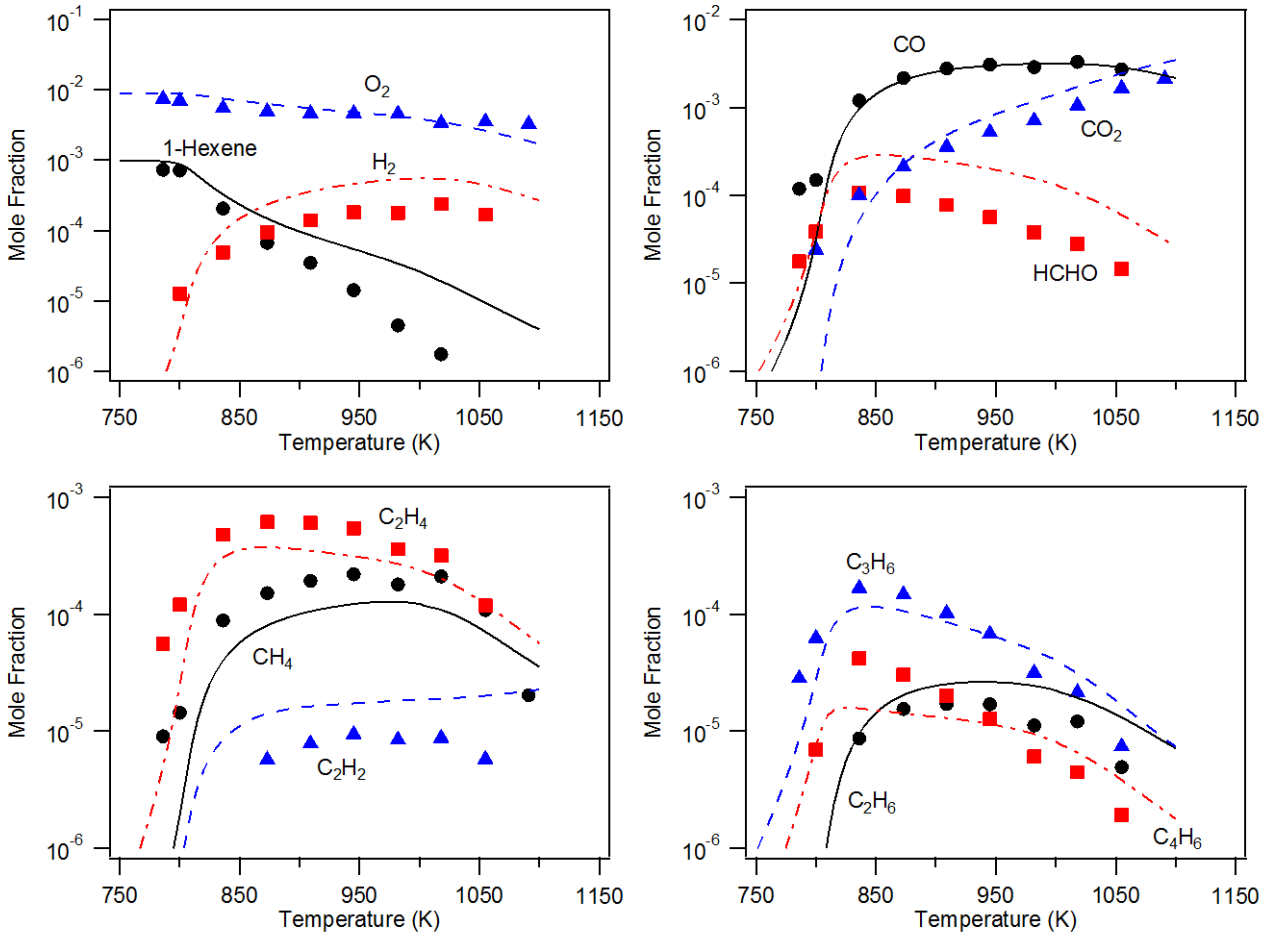

Figure S4: Mole fraction profiles of alkenes and dienes (P = 1 MPa, τ =0.5 s, x_{fuel} = 0.001, x_{O2} = 0.009, x_{N2} = 0.99, φ = 1). Symbols are for experiments and lines for simulations.

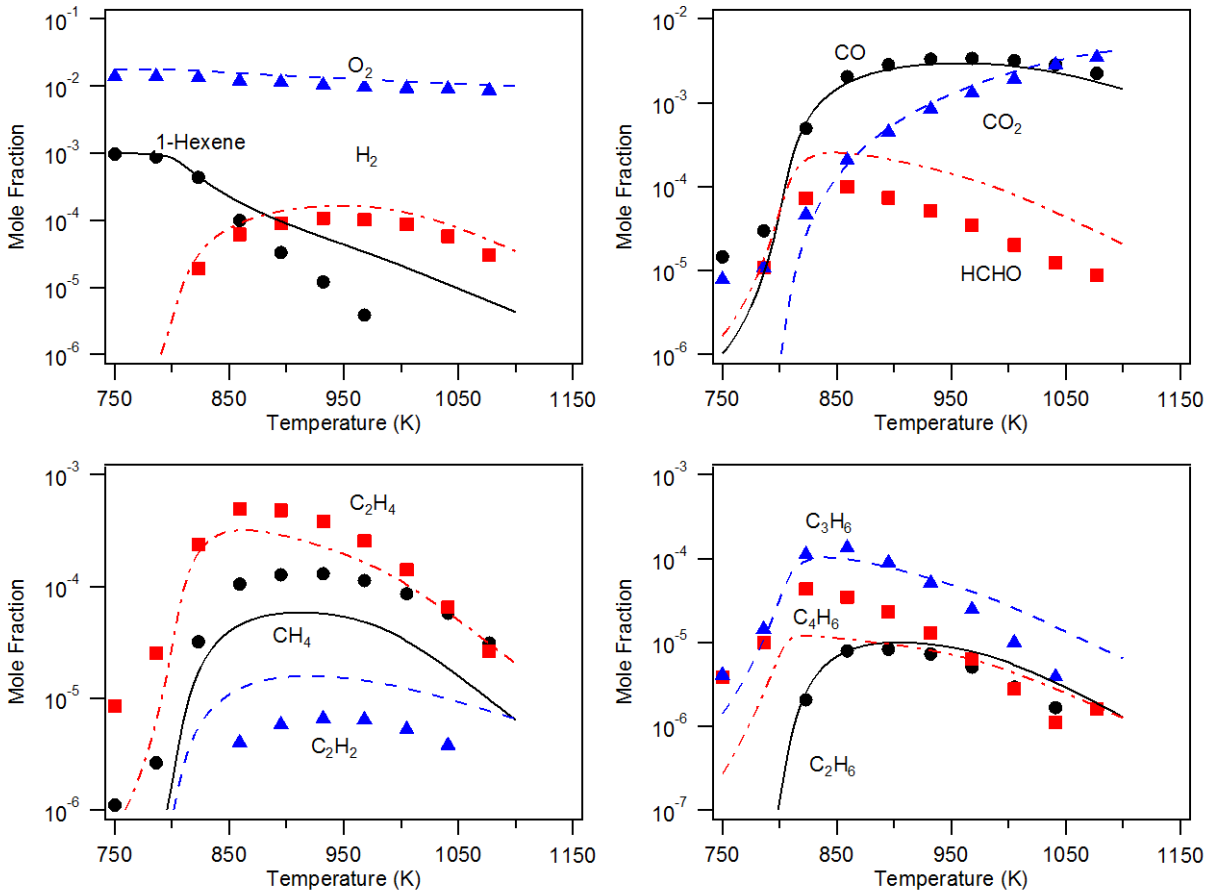

Figure S5: Mole fraction profiles of alkenes and dienes (P = 1 MPa, τ =0.5 s, x_{fuel} = 0.001, x_{O2} = 0.018, x_{N2} = 0.981, φ = 0.5). Symbols are for experiments and lines for simulations.

** High pressure shock tube validation*

Simulations were also conducted to reproduce the ignition delay times measured during the shock tube experiments conducted by Mehl et al. [16] and Yahyaoui et al. [15] at pressure of 10 bar. All shock tube experiments were simulated considering closed homogenous batch reactor on the assumption of constant volume behind the reflected shock wave.

In this study, the inflection point in the computed temperature profile was used to indicate the ignition delay time as did by Mehl et al. [16]. Reasonable agreement is obtained for the shock tube experimental and predicted ignition delay times as shown in Figure S5

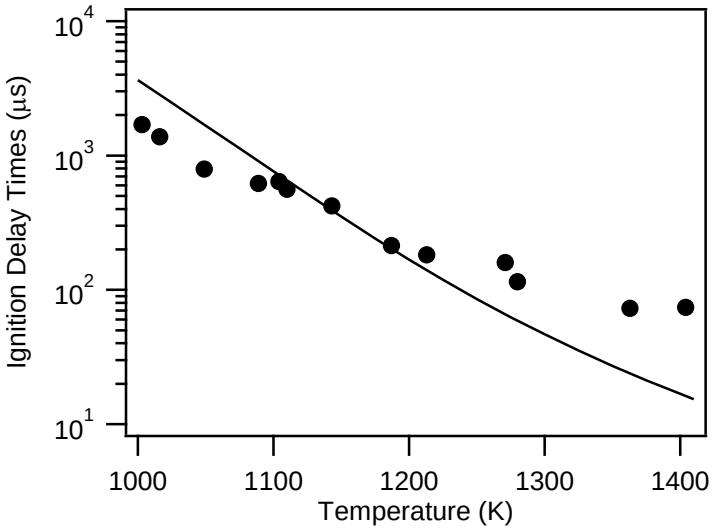

Figure S6: Ignition delay times in a high pressure shock tube at NUI Galway [16]; symbols are for experiments and lines for simulations.

During the shock tube experiments conducted by Yahyaoui et al. [15], the ignition delay time was defined as the 50% of the maximum OH emission. The current model reasonably reproduced the experimental ignition delays at different equivalence ratios despite slight underprediction.

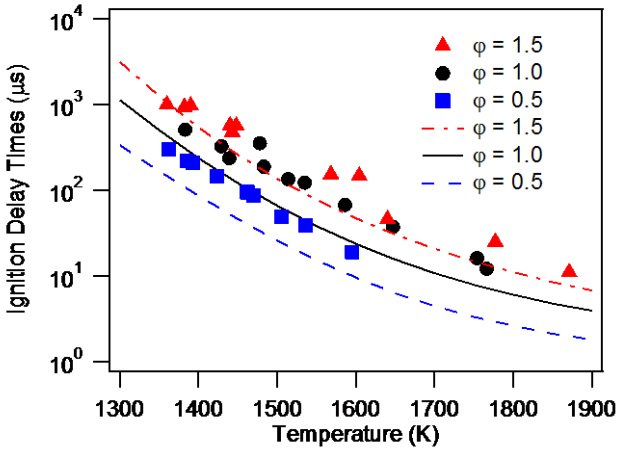

Figure S7: Ignition delay times of high pressure shock tube experiments conducted by Yahyaoui et al. [15]. Symbols are for experiments and lines for simulations.

4/ Reaction flux analysis at 850 K

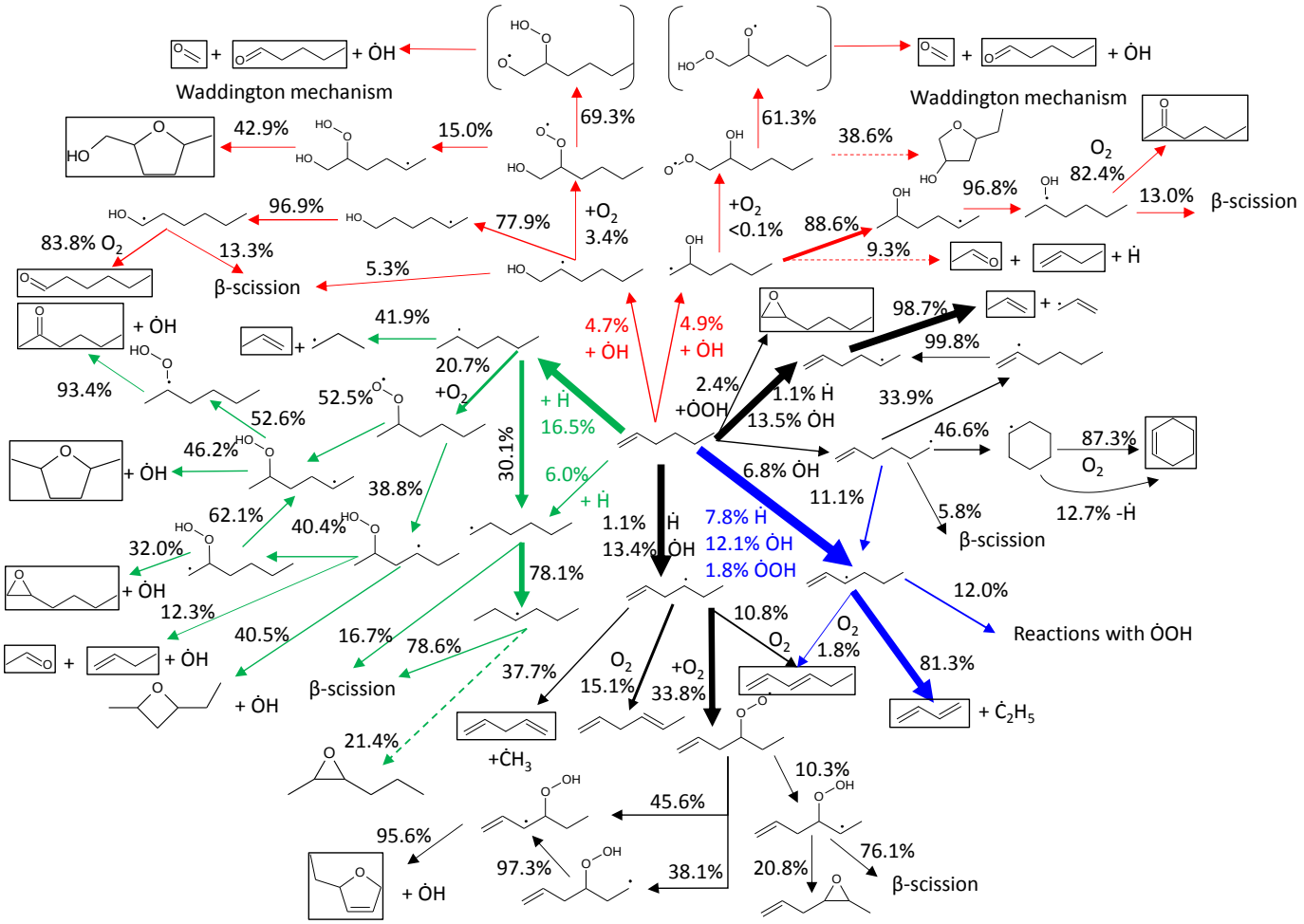

Figure S8: Reaction flux for 1-hexene oxidation computed at 850 K, ϕ = 1; species in boxes were detected during the JSR experiments.

4/ Sensitivity analysis at 650 K

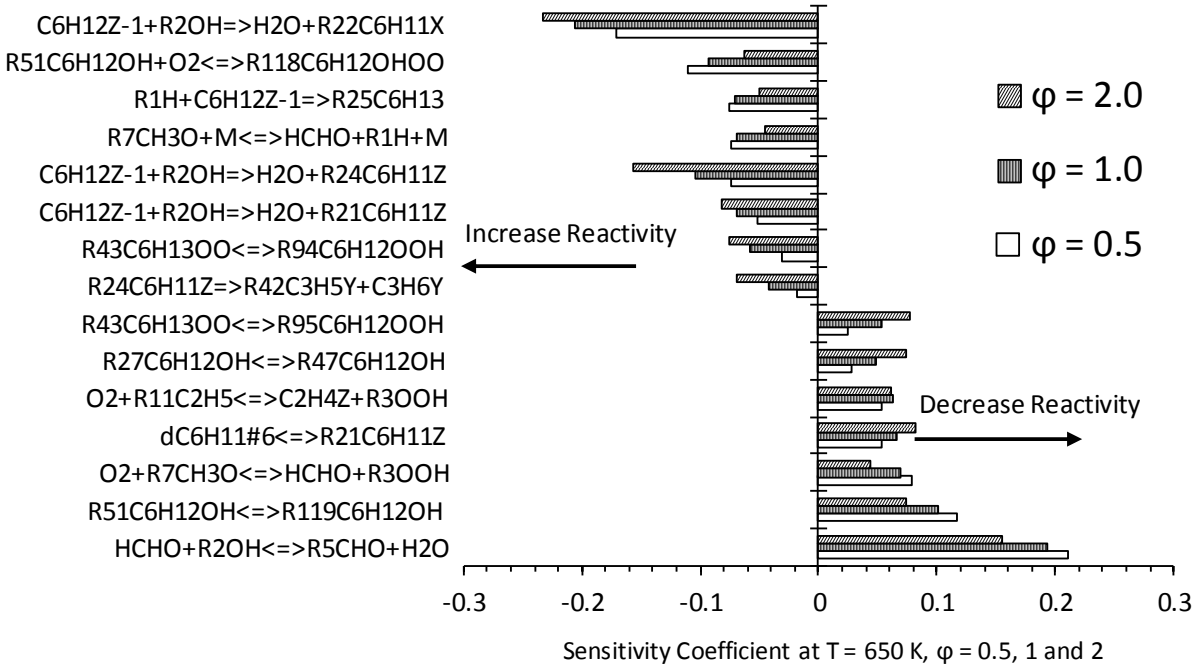

Figure S9: Sensitivity analysis for 1-hexene mole fraction computed at 650 K, and three equivalence ratios (ϕ).

References

[1] A. Rodriguez, O. Herbinet, Z. Wang, F. Qi, C. Fittschen and P. Westmoreland, *Proc. Combust. Inst.*, 36 (2016) in press.

[2] T.A. Cool, K. Nakajima, C.A. Taatjes, A. McIlroy, P.R. Westmoreland, M.E. Law, A. Morel, Proceedings of the Combustion Institute 30 (2005) 1681–1688.

[3] Z. Zhou, L. Zhang, M. Xie, Z. Wang, D. Chen, F. Qi (2010). Rap. Com. Mass Spectrom., 24(9), 1335-1342.

[4] T.A. Cool, K. Nakajima, T.A. Mostefaoui, F. Qi, A. Mcllroy, P.R. Westmoreland, M.E. Law, L. Poisson, D.S. Peterka, M. Ahmed, J. Chem. Phys.119 (2003) 8356–8365.

[5] B. Yang, J. Wang, T.A. Cool, N. Hansen, S. Skeen, D.L. Osborn (2012) Int. J. Mass Spectrom., 309, 118-128.

[6] G.Cooper , J. E. Anderson, C.E. Brion (1996) Chem. Phys., 209(1), 61-77.

[7] T.A Cool, J.Wang, K. Nakajima, C.A. Taatjes, A. Mcllroy, (2005) Int. J. Mass Spectrom., 247(1), 18-27.

[8] L.G. Dodson, L. Shen, J.D. Savee, N.C. Eddingsaas, O. Welz, C.A. Taatjes, D.L. Osborn, S.P. Sander, M. Okumura J. Phys. C chem. A 119, (2015) 1279-1291.

[9] Bobeldijk, M., Van der Zande, W.J., P.G. Kistemaker,. Chem. Phys. 179(2), (1994) 125-130.

[10] J. Wang, B. Yang, T.A. Cool, N. Hansen, T. Kasper (2008). Int. J. Mass Spectrom., 269(3), 210-220.

[11] C. Bahrini, P. Morajkar, C. Schoemaecker, O. Frottier, O. Herbinet, P.-A. Glaude, F. Battin-Leclerc, C. Fittschen, Phys. Chem. Chem. Phys. 15 (2013) 19686–19698.

[12] P. Morajkar, C. Schoemaecker, C. Fittschen, J. Mol. Spectrosc. 281 (2012) 18–23.

[13] P. Macko, D. Romanini, S.N. Mikhailenko, O.V. Naumenko, S. Kassi, A. Jenouvrier, V.G. Tyuterev, A. Campargue, J. Mol. Spectrosc. 227 (2004) 90–108.

[14] A.E. Parker, C. Jain, C. Schoemaecker, P. Szriftgiser, O. Votava, C. Fittschen, Appl. Phys. B Lasers Opt. 103 (2011) 725–733.

[15] M. Yahyaoui, N. Djebaïli-Chaumeix, C.-E. Paillard, S. Touchard, R. Fournet, P.A. Glaude, F. Battin-Leclerc, Proc. Combust. Inst. 30 (2005) 1137–1145.

[16] M. Mehl, W.J. Pitz, C.K. Westbrook, K. Yasunaga, C. Conroy, H.J. Curran, Proc. Combust. Inst. 33 (2011) 201–208.